Entanglement Network of the Polypropylene/Polyamide Interface. 2. Network Generation

Andreas F. Terzis,[†] Doros N. Theodorou,*[,†,‡] and Alexander Stroeks[§]

Department of Chemical Engineering, University of Patras, GR 26500 Patras, Greece; Institute of Chemical Engineering and High-Temperature Chemical Processes, GR 26500 Patras, Greece; and DSM Research, P.O. Box 18, 6160 MD Geleen, The Netherlands

Received June 28, 1999; Revised Manuscript Received October 29, 1999

ABSTRACT: We present a novel algorithm for generating polymer entanglement networks and apply it to polypropylene/polyamide interfaces strengthened with graft copolymers. Our guides for the generation of the polymer network are the configurational distribution functions derived from a self-consistent mean-field lattice theory of the interface. Entanglement points are placed along the contour of each chain at equal distances, corresponding to the experimentally measured molecular weight between entanglements. The spatial distribution of entanglement points in the direction perpendicular to the surface follows the statistical weights of the mean-field theory. Our initial guess for the positions of the entanglement points of each chain parallel to the interface obeys Gaussian statistics. The polymer network created by this procedure is not in equilibrium. Overstretched strands are relaxed by a Monte Carlo method involving moves that preserve the placement in the directions perpendicular to the interface. The equilibrated network is our starting point for the microscopic simulation of fracture phenomena, caused by the application of tensile stress perpendicular to the interface.

1. Introduction

This work is part of an effort to develop theoretical and simulation models for predicting the structure and mechanical properties of polymer/polymer interfaces compatibilized by adding, or forming in situ with appropriate chemical reactions, a diblock copolymer in which each block is miscible with one of the two homopolymers.[1] We focus on the PP/PA6 system compatibilized with the reaction product between PP-*g*-MA (maleic anhydride-functionalized PP) and PA6. This system has been the subject of several experimental studies.[2−4]

As was mentioned in the preceding paper,[5] it is believed that the ultimate mechanical properties of polymeric systems are directly related to entanglements. When each chain in a system of polymeric chains is constrained by point contacts (i.e., entanglements), we say that the system forms a network. In this work we develop a new algorithm in order to generate polymer entanglement networks. The algorithm uses the configurational distribution functions (derived in the preceding paper) in order to properly place polymer chains within the network. To form the network, the positions of the ends and the entanglement points must be known along each chain contour and in three-dimensional space.

In the present work we develop an algorithm that generates networks representative of a PP/compatibilizer/PA6 polymeric interfacial system. In light of the information provided by experimental data, we have considered appropriate to model the PP/PA6 interface by envisioning a crystalline PA6 matrix, treated as an equivalent "solid" substrate, on which the PP chains of the compatibilizer are terminally grafted, extending into a bulk PP phase.[5] To model realistic (i.e., consistent with the characteristics reported in the experimental studies) polymeric interfacial PP/PA6 systems, both the free and grafted PP should have a polydispersity index (PDI) different from unity (usually rather high).

The starting point in order to describe the conformations and concentration profiles of polymeric systems at interfaces is the self-consistent mean-field lattice model (SCF) we described in ref 5 (preceding paper).

In principle, modeling can be performed hierarchically, at different levels of length and time scale. The most fundamental scale is the *atomistic* one. Approaching the system of interest here solely by atomistic modeling would be exceedingly time-consuming and would not be able to provide answers to questions related to terminal mechanical properties. Existing Monte Carlo simulations address only small chain lengths that preclude entanglement formation.[6] A *mesoscopic* model would be more appropriate for our purposes. Systematic procedures to coarse-grain atomistic polymer models into mesoscopic models have already been used successfully.[7] The model we use here is a coarse-grained model. Two levels of coarse-graining are utilized. First, a fully occupied lattice is used to represent the system of interest in the SCF theory. Next, the structural information derived from the SCF theory is used to build an entanglement network model in continuous three-dimensional space. In the lattice model, given a polymer of experimentally known physical properties, we construct a lattice bounded by a flat substrate, the size of each site being equal to the polymer Flory segment. The Flory segment is defined as a length of the polymer chain that is as long as it is wide. It can be estimated once we know the chain geometry as well as the density and the molecular weight.[5] The lattice layers parallel to the surface are numbered from the surface out to the bulk ($z = 1$, ...,

[†] University of Patras.
[‡] Institute of Chemical Engineering and High-Temperature Chemical Processes.
[§] DSM Research.
* To whom correspondence should be addressed at the University of Patras. Phone +3061-997398, FAX +3061-993255, e-mail doros@sequoia.chemeng.upatras.gr.

10.1021/ma991025p CCC: $19.00
Published on Web 02/03/2000

M, layer $z = 0$ being the "wall"). In this model, stiffness is introduced by assigning different energies to different bending angles formed by triplets of Flory segments. (For a cubic lattice, only 0°, 90°, and 180° bending angles are possible.) The bending energies are determined from the characteristic ratio. In our preceding work (ref 5) we have derived results for a variety of monodisperse and polydisperse samples. This lattice mean-field model provided us with a wealth of information regarding the microscopic configurations of the interfacial system. In this context in ref 5 we have calculated the volume fractions of the grafted and free chains, the width of the interfacial region over which free and grafted chains interentangle, and the mean-squared z-component of the end-to-end distance of the grafted chains at various values of the surface grafting density.

In this paper, using the one-dimensional information provided by the SCF theory as a starting point, we develop an algorithm in order to generate three-dimensional networks representative of the interfacial region. In the network, a chain is represented in a very coarse-grained sense as a sequence of two ends and a set of intermediate entanglement points. Two chains come together at an entanglement point. Chain ends and entanglement points are referred to collectively as nodes of the network. Our construction results in a set of nodes for each chain where each node has a specific contour position, spatial location, and pairing with another node if it is an entanglement point. The network is constructed so that all its structural profiles along the z-direction are consistent with the SCF calculation. The SCF results do not impose any restrictions on the extent of the specimen along the x and y directions. The network generated has a finite extent; it could be rather unrealistic close to the free surfaces normal to x and y directions, where the density drops from a finite value to zero, but we avoid to use periodic boundary conditions as they might produce artifacts during the study of ultimate mechanical properties.

Clearly, our use of an entanglement network to represent the polymer stems from our intention to design a computationally efficient approach, capable of handling the length and time scales that govern fracture phenomena. Although the contour length between entanglements is a well-defined quantity (through rheological measurements), entanglements themselves have so far defied a precise molecular definition. In the course of our simulation of deformation to fracture, the topology of the entanglement network will change through the introduction of elementary events (e.g., slippage past an entanglement point, chain rupture) governed by rate expressions and rules that are inspired by the reptation picture of polymer dynamics. Such kinetic Monte Carlo simulations on simplified two-dimensional network models have proved quite successful for addressing the terminal properties of semicrystalline polymers in the bulk (ref 7 of preceding article), thus providing justification for the use of representations cast in terms of localized entanglement points for modeling the large-scale deformation and fracture of dense systems of interpenetrating chains. A currently very active area of research aims at a precise definition of entanglements in polymer melts through topological analysis of well-equilibrated long-chain atomistic configurations[8] or through Brownian dynamics simulations of coarse-grained models in which chain uncrossability is imposed.[9] Thus, it is likely that modeling hierarchies going all the way from detailed atomistic modeling to entanglement network modeling will be available soon.

Typical sizes of the network system generated here are on the order of 0.1−0.2 μm along each direction. The number of chains can be as high as 20 000 and the number of entanglement points as high as 130 000.

2. Network Generation

General Assumptions. A strand is the portion of a chain connecting two interior points or an interior point with an end point. Entanglement points connected by more that one strand are not allowed. In addition, loops formed by a strand connecting an entanglement point to itself are not allowed.

Once we have the configurational distribution functions of the grafted and the free homopolymer, we have adequate information to attempt to construct an entanglement network in three-dimensional space, representing the polypropylene phase. In a first attempt to create an entanglement network, the entanglement points can be placed along the chain contour assuming that interentanglement spacings follow a simple distribution. The simplest choice is to place the entanglement points at equal distances along the chain contours. The distance between consecutive entanglement points has been specified by means of the entanglement molecular weight M_e, as it is measured by the rubbery plateau of the shear stress relaxation modulus.[10] For the first and last entanglement point some constraints are imposed. For both terminal entanglement points of a free chain and for the entanglement point nearest the free end of the grafted chains, the distance along the contour between entanglement and chain end must not be closer than $M_e/3$. Entanglement points on the other end of the grafted chains can be arbitrarily close to the grafting point of the chain. Entanglement points chosen along the chain contour are placed in space according to the chain configurational distribution functions. In the direction perpendicular to the flat substrate, the entanglement points will be placed according to the results of the SCF model, while in the directions parallel to the substrate they will be placed according to Gaussian statistics. Although the network generation essentially takes place in continuous three-dimensional space, it is convenient to use the discretization invoked by the SCF theory in the form of a Flory lattice.

The theory of rubber elasticity predicts a relationship between the shear modulus and the concentration of network strands.[10] Provided we have experimental values of the plateau modulus of the molten polymer, we can use this relationship in order to evaluate the molecular weight M_e. Unfortunately, there are no experimental values for the plateau modulus of isotactic polypropylene. Lacking those for isotactic, we use the atactic values.[11] We suspect that this assumption might not be too unsatisfactory, as atactic and isotactic PP have similar densities and characteristic ratios.[12,13] With this assumption, we carry out our network construction with a value of $M_e = 6$ kg/mol (~60 Flory segments). Moreover, in the PP/PA6 interfacial system the value for M_e should be different, as all grafted and some free chains are more ordered along the direction perpendicular to the interface. However, as a first approximation we use the bulk value because of lack of an alternative approach.

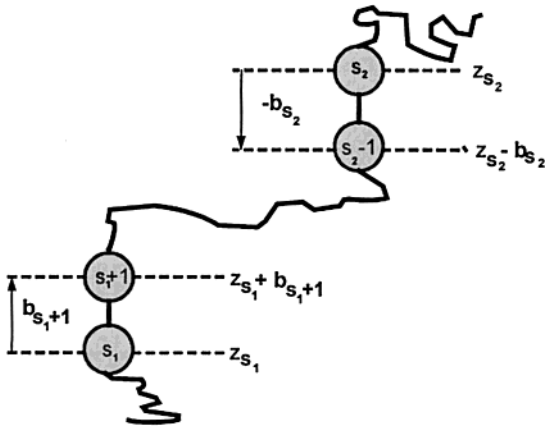

Figure 1. Definition of $G^{b_{s2},b_{s1+1}}(z_{s_2},s_2;z_{s_1},s_1)$. From $G(z)$'s we construct a statistical weight, $G^{b_{s2},b_{s1+1}}(z_{s_2},s_2;z_{s_1},s_1)$, for the chain portion between segments s_1 and s_2, inclusive, with $s_1 < s_2$, such that segment s_1 is in layer z_{s_1} and is connected to segment $(s_1 + 1)$ through a bond of bond vector b_{s_1+1}, while segment s_2 is in layer z_{s_2} and is connected to segment $(s_2 - 1)$ through a bond of bond vector b_{s_2}.

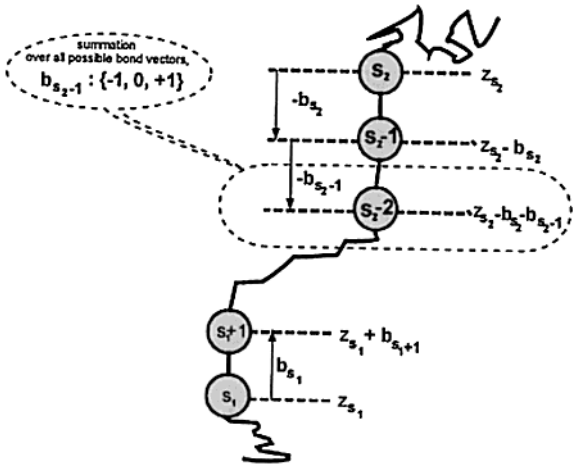

Figure 2. Schematic explanation of the recursion relation: $G^{b_{s2},b_{s1+1}}(z_{s_2},s_2;z_{s_1},s_1) = G(z_{s_2},s_2)\lambda_{|bs_2|}\sum_{b_{s2-1}}\tau_{b_{s2-1}b_{s2}}G^{b_{s2-1},b_{s1+1}}(z_{s_2} - b_{s_2},s_2 - 1;z_{s_1},s_1)$ which is a generalization of eq 4 of ref 5.

Placement along the *z*-Axis. Our starting points are the segment weighting factors ($G(z)$) of the SCF theory. From $G(z)$'s we construct a statistical weight, $G^{b_{s2},b_{s1+1}}(z_{s_2},s_2;z_{s_1},s_1)$, for the chain portion between segments s_1 and s_2, inclusive, with $s_1 < s_2$, such that segment s_1 is in layer z_{s_1} and is connected to segment $(s_1 + 1)$ through a bond of bond vector b_{s_1+1}, while segment s_2 is in layer z_{s_2} and is connected to segment $(s_2 - 1)$ through a bond of bond vector b_{s_2} (see Figure 1). We easily identify the end segment distributions, used in SCF theory, as

$$G^{b_s}(z_s,s|1) = \sum_{z_{s_1}}\sum_{b_{s_1+1}} G^{b_{s2},b_{s1+1}}(z_{s_2} = z_s,\, s_2 = s;\, z_{s_1},\, s_1 = 0)$$

and

$$G^{b_{s+1}}(z_s,s|r) = \sum_{z_{s_2}}\sum_{b_{s_2}} G^{b_{s2},b_{s1+1}}(z_{s_2},\, s_2 = r + 1;\, z_{s_1} = z_s,\, s_1 = s)$$

The function $G^{b_{s2},b_{s1+1}}(z_{s_2},s_2;z_{s_1},s_1)$ obeys the recursion relation (see Figure 2):

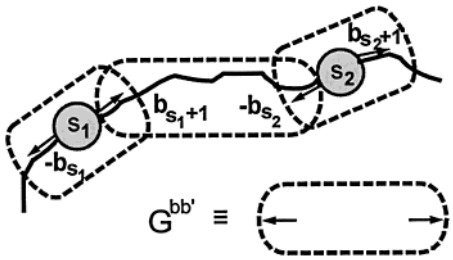

Figure 3. Schematic explanation of the recursion relation $G^{(2)}(\{(z_{s_1},s_1),(z_{s_2},s_2)\}) = \sum_{b_{s1}}\sum_{b_{s1+1}}\sum_{bs2}\sum_{b_{s2+1}}G^{-1}(z_{s_1},s_1)G^{-1}(z_{s_2},s_2)\tau_{b_{s1}b_{s1+1}}\tau_{b_{s2}b_{s2+1}}G^{b_{s1+1}b_{s1}}(z_{s_1},s_1;z_{s_1},s_1)G^{b_{s2}b_{s1+1}}(z_{s_2},s_2;z_{s_1},s_1)G^{b_{s2+1}b_{s2}}(z_{s_2},s_2;z_{s_2},s_2)$.

Figure 4. Schematic explanation of the recursion equation $G^{(3)}(\{(z_{s_1},s_1),(z_{s_2},s_2),(z_{s_3},s_3)\}) = \sum_{b_{s1}}\sum_{b_{s1+1}}\sum_{b_{s2}}\sum_{b_{s2+1}}\sum_{b_{s3+1}}\tau_{b_{s1}b_{s1+1}}\tau_{b_{s2}b_{s2+1}}\tau_{b_{s3}b_{s3+1}}G^{-1}(z_{s_1},s_1)G^{-1}(z_{s_2},s_2)G^{-1}(z_{s_3},s_3)G^{b_{s1+1}b_{s1}}(z_{s_1},s_1;z_{s_1},s_1)G^{b_{s2}b_{s1+1}}(z_{s_2},s_2;z_{s_1},s_1)G^{b_{s3}b_{s2+1}}(z_{s_3},s_3;z_{s_2},s_2)G^{b_{s3+1}b_{s3}}(z_{s_3},s_3;z_{s_3},s_3)$.

$$G^{b_{s2},b_{s1+1}}(z_{s_2},s_2;z_{s_1},s_1) = G(z_{s_2},s_2)\lambda_{|bs_2|} \times \sum_{b_{s2-1}}\tau_{b_{s2-1}b_{s2}}G^{b_{s2-1},b_{s1+1}}(z_{s_2} - b_{s_2},\, s_2 - 1;\, z_{s_1},\, s_1) \quad (1)$$

which is a generalization of eq 4 of ref 5, but now the initial condition involves only two segments, such that $s_2 = s_1 + 1$,

$$G^{b_{s1+1},b_{s1+1}}(z_{s_1+1},s_1{+}1;z_{s_1+1} - b_{s_1+1},s_1) = G(z_{s_1+1},s_1 + 1)\lambda_{|b_{s1+1}|}G(z_{s_1+1} - b_{s_1+1},s_1) \quad (2)$$

By properly (i.e., using the correct Boltzmann factors) summing the previously defined statistical weights, we calculate the statistical weights $G^{(m)}(\{z_{s_k},s_k\})$ for a chain to have m of its segments, with indices s_k ($k = 1, 2, ..., m$), ordered such that $s_1 < s_2 < ... < s_k < ... < s_m$, positioned in the z-direction according to $\{z_{s_k},s_k\}$. These statistical weights are given by

$$G^{(m)}(\{z_{s_a},s_a\}) = \sum_{b_{s_1}}\sum_{b_{s_1+1}}\cdots\sum_{b_{s_a}}\sum_{b_{s_a+1}}\cdots\sum_{b_{s_m}}\sum_{b_{s_m+1}} G^{b_{s1+1}b_{s1}}(z_{s_1},s_1;z_{s_1},s_1) \times \prod_{a=1}^{m-1}\tau_{b_{sa}b_{sa+1}}G^{-1}(z_{s_a},s_a)G^{b_{s(a+1)}b_{sa+1}}(z_{s_{a+1}},s_{a+1};z_{s_a},s_a) \times \tau_{b_{sm}b_{sm+1}}G^{-1}(z_{s_m},s_m)G^{b_{sm+1}b_{sm}}(z_{s_m},s_m;z_{s_m},s_m) \quad (3)$$

Figures 3 and 4 show which $G^{b_{sb},b_{sa+1}}(z_{s_b},s_b;z_{s_a},s_a)$ contribute to $G^{(2)}$ (statistical weights for pairs of segments) and $G^{(3)}$ (statistical weights for triplets of segments).

The $G^{(2)}$ statistical weights are used in order to place along the z-axis the two end segments of a chain composed of r segments. In this special case, $s_1 = 1$ and $s_2 = r$. Actually, as $G^{(m)}$ are weights, it is necessary to normalize them in order to define absolute probabilities. The normalization is performed by dividing by the sum of $G^{(m)}$ over all positions available to the m distinct segments of the chain.

Thus, the placement of the end segments is performed according to the probability:

$$p^{(2)}(\{(z_1,1)(z_r,r)\}) = \frac{G^{(2)}(\{(z_1,1)(z_r,r)\})}{\sum_{z_1,z_r} G^{(2)}(\{(z_1,1)(z_r,r)\})} \quad (4)$$

The placement of the next (intermediate) segment s at position z can be performed following a conditional probability, derived by applying Bayes' rule [$p(A/B) = p(A\cap B)/\sum_B p(A\cap B)$] for $A \equiv (z,s)$ and $B \equiv (\{(z_1,1)(z_r,r)\})$. Actually, as we have a ratio of probabilities, we can replace the probabilities with statistical weights and derive a simpler conditional probability for placing any segment between two segments already placed:

$$p^{(3)}(\{(z_{s_k},s_k)|\{(z_{s_1},s_1),(z_{s_r},s_r)\}) = \frac{G^{(3)}(\{(z_{s_1},s_1),(z_{s_k},s_k),(z_{s_r},s_r)\})}{\sum_z G^{(3)}(\{(z_{s_1},s_1),(z,s_k),(z_{s_r},s_r)\})} \quad (5)$$

For each chain, each one of the interior segments s_l is placed along the z-axis in a randomly chosen order, according to the probabilities

$$p^{(m)}(\{(z_{s_l},s_l)|\{(z_{s_1},s_1),\ldots,(z_{s_k},s_k),\ldots,(z_{s_r},s_r)\}) = \frac{G^{(m)}(\{(z_{s_1},s_1),\ldots,(z_{s_k},s_k),\ldots,(z_{s_l},s_l),\ldots,(z_{s_r},s_r)\})}{\sum_z G^{(m)}(\{(z_{s_1},s_1),\ldots,(z_{s_k},s_k),\ldots,(z,s_l),\ldots,(z_{s_r},s_r)\})}$$

where $m - 1$ is the number of already placed interior segments or ends.

The procedure for placing end points and entanglement nodes for each chain of each chain type can thus be summarized as follows.

1. Since the normalization for two segments is relatively simple, we start with the end segments of the chain, placing them in the z-direction according to the probability $p^{(2)}(\{(z_1,s_1),(z_r,s_r)\})$ (eq 4).

2. After placing the ends, an interior segment s_k of the chain, chosen randomly among the prospective entanglement points defined along the contour, is placed according to Bayes' rule (eq 5), using the conditional probability distribution derived from the three-segment statistical weights, $p^{(3)}((z_k,s_k)|\{(z_1,s_1),(z_r,s_r)\})$.

3. The next interior segment s_l, again chosen randomly, is placed according to Bayes' rule, using the conditional probability distribution derived from the four segment statistical weights, $p^{(4)}((z_l,s_l)|\{(z_1,s_1),(z_k,s_k),(z_r,s_r)\})$.

4. We proceed in a similar manner using conditional probabilities, until we place all segments chosen to represent entanglement nodes.

Make Even Procedure. Having placed the nodes in the z-direction, the discretization of space being such that the closest distance of nodes along the z-direction is equal to the Flory segment size l_F, we check each layer to ensure that it contains an even number of entanglement nodes. In case this is not true for a layer, an entanglement nodal point is moved to a nearby layer with odd number of entanglement nodes, such that both layers have an even number of entanglement nodes. This procedure is performed sequentially, layer by layer. If the last layer examined contains an odd number of nodes, then we remove a node from that layer. The final result is that all layers contain an even number of entanglement nodal points. The procedure by which we move a node from one layer to another is usually quite time-consuming, as the new position of the node is required to have an SCF probability at least equal to that of the old position.

Placement of Nodes in the *x* and *y* Directions. The next step is to place the nodes in the x and y directions. The first node of each chain (which is an end of the chain) is placed randomly within its layer at position (x_1,y_1). From this initial node, all other nodes of the chain are placed sequentially within their respective z-layers, following the contour, according to a truncated Gaussian distribution. The wings of the Gaussian distribution are truncated with appropriate renormalization in order to avoid placement of the nodes such that the contour length of the strand in between exceeds the spatial distance between the nodes (i.e., in order to avoid overstretched strands). In addition, nodes are not placed outside the finite network window. The sampling procedure of the truncated Gaussian follows a rejection technique.[14] The choice of a distribution similar to Gaussian is reasonable, as in the x and y directions no forces act to deform the chains away from their random coil behavior. If a node, s_1, is placed randomly within its layer (i.e., layer z_1) at position (x_1,y_1), then the next node, s_2, is placed at a position (x_2,y_2) within layer z_2 (already known from the z-placing procedure) according to the probability density $p(x_2,y_2) = p_x(x_2)p_y(y_2|x_2)$, where

$$p_x(x_2) = \left(\frac{3}{2\pi N_K {l_K}^2}\right)^{1/2}\left[\mathrm{erf}\left\{\left(\frac{3}{2N_K {l_K}^2}\right)^{1/2}\tilde{x}_{12}\right\}\right]^{-1} \times \exp\left[-\frac{3(x_2-x_1)^2}{2N_K {l_K}^2}\right], \quad \text{for } -\tilde{x}_{12}+x_1 \le x_2 \le \tilde{x}_{12}+x_1$$

$$0, \quad \text{for } x_2 \le -\tilde{x}_{12}+x_1 \text{ and } x_2 \ge \tilde{x}_{12}+x_1$$

with

$$N_K = (s_2 - s_1)\frac{l_F}{l_K}, \quad \tilde{x}_{12} = \sqrt{(s_2-s_1)^2 - (z_2-z_1)^2}\, l_F \quad (6)$$

$$p_y(y_2|x_2) = \left(\frac{3}{2\pi N_K {l_K}^2}\right)^{1/2}\left[\mathrm{erf}\left\{\left(\frac{3}{2N_K {l_K}^2}\right)^{1/2}\tilde{y}_{12}\right\}\right]^{-1} \times \exp\left[-\frac{3(y_2-y_1)^2}{2N_K {l_K}^2}\right], \quad \text{for } -\tilde{y}_{12}+y_1 \le y_2 \le \tilde{y}_{12}+y_1$$

$$0, \quad \text{for } y_2 \le -\tilde{y}_{12}+y_1 \text{ and } y_2 \ge \tilde{y}_{12}+y_1$$

with

$$\tilde{y}_{12} = \sqrt{{\tilde{x}_{12}}^2 - (x_2-x_1)^2} \quad (7)$$

In eqs 6 and 7, l_K is the Kuhn length of the chain.

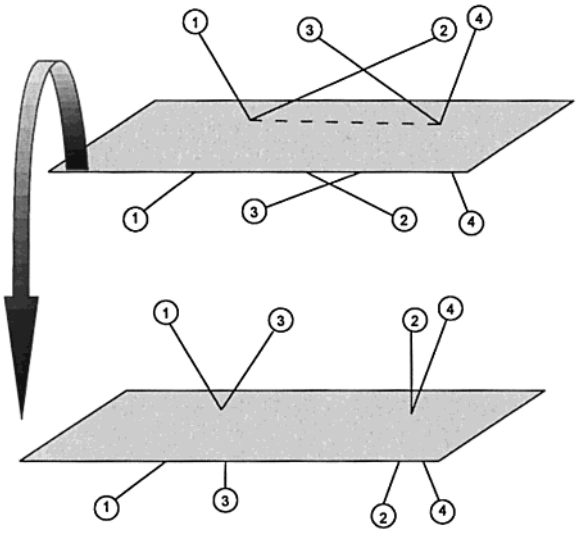

Figure 5. Swapping of chains between entanglement points.

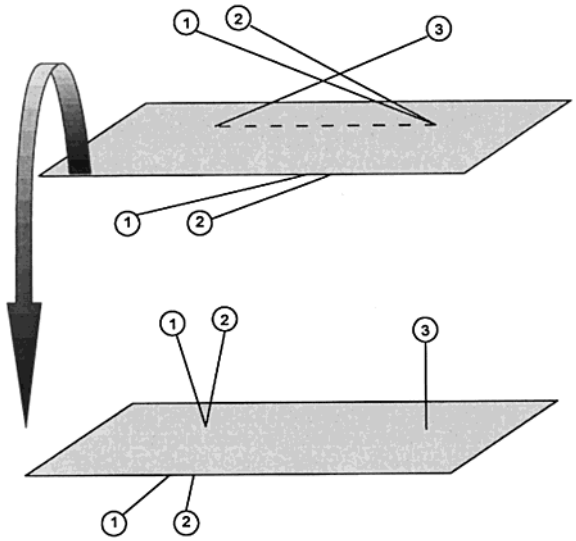

Figure 6. Swapping of an entanglement point and an end point.

This procedure is continued until all nodes of all chains have been placed.

Pairing of Entanglement Nodes. After placing all the available nodes, the entanglement nodes are paired within layers to form entanglements. Within a layer, we choose nodes for pairing in random order. We pair the nearest unpaired nodes, avoiding double connections and loops. The spatial position of two entanglement nodes after pairing is chosen as the midpoint of the line connecting them within the layer. We repeat this procedure until all entanglement nodes have been paired. By this procedure, the last few nodes paired in a layer may lead to overstretched strands. This overstretching occurs because the nearest nodes that remain unpaired may be very far from each other toward the end of the pairing procedure.

Relaxation. We need to relax all overstretched strands. The relaxation of overstretched strands follows a Monte Carlo (MC) procedure. The in-layer moves utilized in this procedure are the following: (a) Swapping of chains between entanglements. This changes pairing and spatial positions; see Figure 5. In this move two chains (2 and 3 in the figure) and four strands are involved. (b) Swapping the position of an entanglement point and an end (Figure 6). In this move three chains (1, 2, and 3) and five strands are involved. (c) Swapping the position of two chain ends (Figure 7).

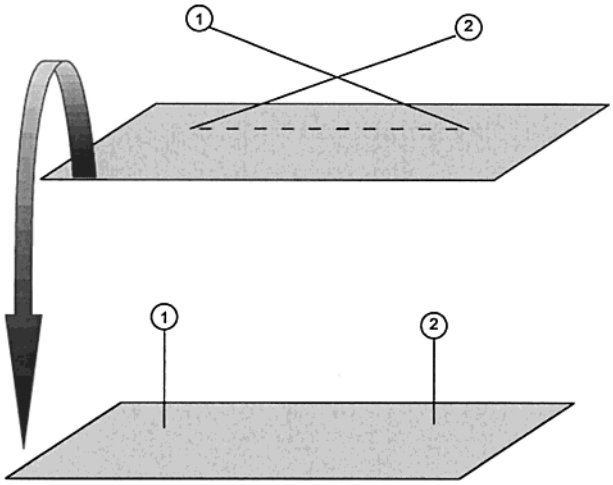

Figure 7. Swapping of two end points.

According to the Metropolis MC algorithm we use for overstretched strand relaxation, attempted moves are accepted with probability $\min(1,\exp(-\Delta U))$ where ΔU is the change in the elastic free energy brought about by the MC move. The elastic free energy change equals the sum of the changes in stretching free energy of all strands involved in the move. The stretching free energy for each strand is calculated by assuming that strands behave as Gaussian entropy strings. For example, for move type b there are five strands involved. The layer in which we perform a move and the points involved in the move are selected at random from all those available in the system. The frequency with which a move type is attempted is proportional to the number of entities in the system that can participate in the move. In a system with u entanglement points and w ends, the relative attempt frequencies are as follows: move type a, $2u/T$; move type b, $(u + w)/T$; move type c, w/T (where $T = 3u + 2w$).

This relaxation procedure is really necessary in order to achieve "random coil" configurations in the bulk region of the free chains.

Density of Entanglement Points. We are mainly interested in investigating the region where grafted and free chains interentangle, as this region is most important for studying mechanical properties and adhesion. We study the effect of the surface density of grafted chains on the surface density of entanglements between free and grafted chains. These entanglements would be expected to be primarily responsible for adhesion at the interface. The calculation of the entanglement density is a simple counting procedure.

As the relaxation procedure does not change the z coordinates of the nodal points and as the pairing of the entanglement nodes is mainly random (as described in the pairing procedure), we expect (and actually show, see results) that random mixing of different types of entanglements is a legitimate approximation. With that assumption, if N_A and N_B are the numbers of entanglement nodes of chains of type A and type B, respectively, in layer z, the numbers of AA, AB, and BB entanglements in that layer are given by

$$N_{AA} = \frac{N_A(N_A - 1)}{2(N_A + N_B - 1)}$$

$$N_{BB} = \frac{N_B(N_B - 1)}{2(N_A + N_B - 1)} \quad (8)$$

$$N_{AB} = N_{BA} = \frac{N_A N_B}{N_A + N_B - 1}$$

If the random mixing approximation holds, it is possible to estimate the entanglement density before the relaxation procedure.

Furthermore, because the procedure by which we assign to each layer (z) an even number of entanglement nodes is rather time-consuming and because after that procedure the number of nodes per layer is not usually very different (each layer changes its number of entanglement nodes by at most one node), it is satisfactory to estimate the total number of entanglements between chains of different types before this procedure.

Reverse Mapping of Network Structure onto the SCF Representations. It is useful to check whether, after the placement of nodal points along the z-direction, the z-projection of the network specimen agrees with the SCF one-dimensional distribution functions used for its generation. To make this comparison at a Flory segment level, we need to account for the intermediate (between adjacent nodal points) segments of each chain. To do this, we invoke a density distribution to describe the position (along the z-direction) of the intermediate segments in a strand whose ends are fixed in space.

Under the assumption that the strands between fixed successive nodal points (s_1, s_2) along the contour are Gaussian, the probability density for finding a segment s in position $\vec{R}$ in space is given by the expression

$$p(s,\vec{R}|s_1,\vec{R}_{s_1}s_2,\vec{R}_{s_2}) = \left(\frac{3c_s}{2\pi}\right)^{3/2} e^{-(3/2)c_s(\vec{R}-\vec{R}_m)^2} \quad (9)$$

If n specifies the number of Kuhn segments between the two tethered end points of the strand, the parameter c_s is just $n/[(n - s)sl_K^2]$ and $\vec{R}_m = [(n - s)\vec{R}_{s_1} + s\vec{R}_{s_2}]/n$.

Since only the density along the z-direction is needed, the integral of the probability density expression of eq 9 over the entire range of the x and y coordinates is used.

The Gaussian approximation is best for large n and $|\vec{R}_{s_1} - \vec{R}_{s_2}|$ small compared to full extension (nl_K). From the statistics of the Kuhn segments we can derive the respective distributions of the Flory segments (i.e., we use eq 9 with s, n representing equivalent Kuhn segments $s[n] \equiv s_K[n_K] = s_F(l_F/l_K)[n_F\ (l_F/l_K)]$).

The probability density for finding a segment s in layer z (i.e., the integral over x and y of eq 9) is

$$p(s,z|s_1,z_{s_1},s_2,z_{s_2}) = \left(\frac{3c_s}{2\pi}\right)^{1/2} e^{-(3/2)c_s(z - z_m(s))^2} \quad (10)$$

where

$$z_m(s) = \frac{(n - s)z_{s_1} + sz_{s_2}}{n}$$

Equation 10 can be used to calculate the intermediate segment density.

The volume fractions can be found by means of the following expression:

$$\phi(s,z) = \sum_s \sum_{(s_1,s_2)} p(s,z|s_1,z_{s_1},s_2,z_{s_2}) l_F \quad (11)$$

where the summation is over the contours of all strands (s_1,s_2) realized in our network. Following this procedure, the segment volume fraction profiles are found and compared to the SCF results. For the end segment volume fraction profiles, a variant of eq 11 is used, wherein the probability density of the terminal segments of singly tethered strands is summed over all such strands. Volume fraction profiles are accumulated separately for free and grafted chains.

Results

SCF and Network Profiles. We start our investigations by creating entanglement networks for monodisperse samples with chain lengths 400 Flory segments for the grafted chains and 600 Flory segments for the free chains. We distinguish each sample according to its surface density (see Table 1). The values used in our calculations correspond to low (0.04 nm^{-2}), intermediate (0.20 nm^{-2}), and high surface density (0.50 nm^{-2}). We choose the number of sites per layer such that the surface density of the network system be as close as possible to the input surface density used in the SCF model.

In all cases the extent of the network in the z-direction is chosen such that we include enough chains of both types with the proper number- and weight-average molecular weights (i.e., the ones used in the SCF calculation). Usually the cases of very low surface density of the grafted chains are the most difficult to realize, as the generation of a huge network (at least in the x- and y-directions) is necessary.

Although the network generation seems straightforward, difficulties arise from the fact that most procedures used for the generation of the network are rather time-consuming. In Table 2 the CPU time spent in each part of the generation procedure is given for the monodisperse samples reported in Table 1.

Most time-consuming are the procedures in which we try to make the number of chains even (in order to create pairs of entanglement nodes in each layer) and the relaxation procedure. We have observed that the latter consumes most of the overall CPU time for the largest (in number of chains) networks. In the most general case of polydisperse samples, the network generation is much more time-consuming. (For example, the generation of a representative polydisperse sample of PDI equal to 4.8 for the free chains and 2.7 for the grafted chains, following a logarithmic normal (lognorm) distribution, requires several days of CPU time on a Silicon Graphics Origin 200 workstation.)

In Figure 8a−c we show the entanglement density profiles determined after generation and relaxation of the network. The dotted line indicates the entanglement density in bulk PP. If M_n is the number-average molecular weight, M_e is the molecular weight between entanglements, $M_{\text{end strands}}$ is the molecular weight of the two end strands in each chain, and ρ is the mass density of bulk PP, an estimate of the entanglement density ($\bar{\rho}_e$) in the bulk is obtained by the expression

$$\bar{\rho}_e = \frac{N_A\rho}{2M_n}\frac{M_n + M_e - M_{\text{end strands}}}{M_e} \quad (12)$$

Table 1. Sizes of Monodisperse Specimens with Chain Lengths 400 Flory Segments for the Grafted Chains and 600 Flory Segments for the Free Chains

surface density (nm^{-2}) of grafted chains	system size {*x*, y, *z*}	total no. of chains	total no. of grafted chains
0.04	1303 Å × 1303 Å × 727 Å	9472	679
0.20	1212 Å × 1212 Å × 1212 Å	11375	2938
0.50	1212 Å × 1212 Å × 1515 Å	19116	7345

Table 2. Fraction of the CPU Time Spend in Each Procedure during Entanglement Network Generation

	fraction of CPU time [%]		
procedure	$\sigma = 0.04$ nm^{-2}	$\sigma = 0.20$ nm^{-2}	$\sigma = 0.50$ nm^{-2}
z placement	12	10	6
make even	20	20	23
xy placement, pairing	8	7	2
relaxation	60	63	69

In Figure 8 we show two dotted lines, as we have two estimates of the average entanglement density: one for the grafted and one for the free chains. For the grafted chains we obtain 0.033 47 nm^{-3}, and for the free chains we obtain 0.037 19 nm^{-3}. In both cases we assume $\rho =$ 0.743 g/cm^3. The difference arises mainly from the difference in the molecular weight of the end strands. In selecting nodal points along the chain contours, it is assumed that the grafted end strand of a grafted chain can be arbitrarily small, while the free end strand of a grafted chain and of the two end strands of a free chain are at least one-third of M_e long.

For the sample with the lowest surface density we observe (Figure 8a) a flat distribution of entanglement points, except in the last layers at the edge of the specimen ($z >$ 1100 Å). The decay observed in these layers is to be expected from the procedure we follow to construct our network. In placing entanglement points along the *z*-direction, we always start with the end points of each chain, and then we place an entanglement point, then a second, until we place all entanglement points. In the last layers we miss all entanglement points that belong to chains that have one or both of their end points in layers $z > M$. A practical solution to this problem is to cut off the decaying profile at the edge, ending up with a smaller (last layer $<M$) network but with proper entanglement density profile, corresponding to an almost fully occupied three-dimensional lattice. The same system size effect is observed for the other two samples of higher surface densities. Moreover, the entanglement density profiles of these samples show more structure. A significantly lower density of the number of entanglement points is observed in the first layers. This is a consequence of the expected (see end-to-end distance results of ref 5) and actually observed tendency of the grafted chains to orient perpendicular to the surface. This effect is more pronounced in the sample with the highest surface density of grafted chains. For this sample, in addition, we observe a lowering of the density of entanglement points at an intermediate distance from the interface (around $z =$ 400 Å). To understand the physical reasons that drive the system toward this behavior, we need to distinguish the entanglement points on the basis of the types of the chains involved. This is done in Figure 9a−c. For the low surface density sample (Figure 9a) we observe that, close to the surface, the density of entanglement points is mainly due to entanglements between grafted and

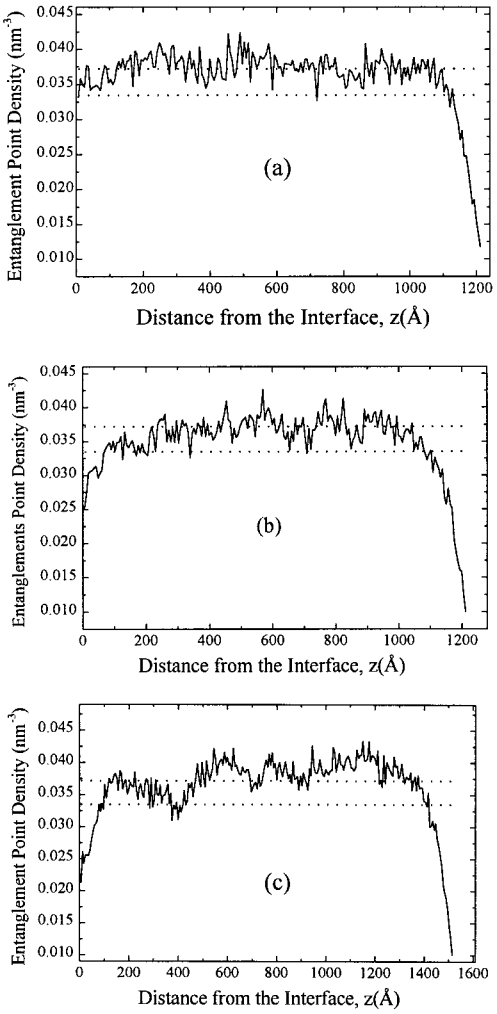

Figure 8. Entanglement density profile determined after generation and relaxation of the network in specimens consisting of monodisperse free chains of length 600 Flory segments for the free chains and 400 Flory segments for the grafted chains. Each plot corresponds to a different surface density of grafted chains: (a) $\sigma = 0.04$ nm^{-2}, (b) $\sigma = 0.20$ nm^{-2}, and (c) $\sigma = 0.50$ nm^{-2}. The lower dotted line (at 0.033 47 nm^{-3}) in all plots designates the entanglement point density of a bulk PP sample with average chain length of 400 Flory segments, and the upper dotted line (at 0.037 19 nm^{-3}) designates the entanglement point density of a bulk PP sample with average chain size of 600 Flory segments. The average strand size between adjacent entanglement points is 60 Flory segments.

free chains and between pairs of free chains. The density of entanglements between pairs of grafted chains is lower and decreases in a systematic way as we depart from the surface. As we move to larger distances from the interface, the contribution is mainly from entanglements between free chains. At even larger distances, where grafted chains are absent, only entanglements among free chains are responsible for the total density of entanglement points. As we see from the other two plots (b and c) and as expected, the same behavior is observed for the two specimens of higher surface density. The specimen with an intermediate surface density exhibits an increased contribution from the grafted chains. Actually, the region close to the interface is practically occupied only by entanglement points between grafted chains. Now, the region from the interface up to the point where no entanglements between pairs of grafted chains exist is much more extended. A similar topology is observed for the speci-

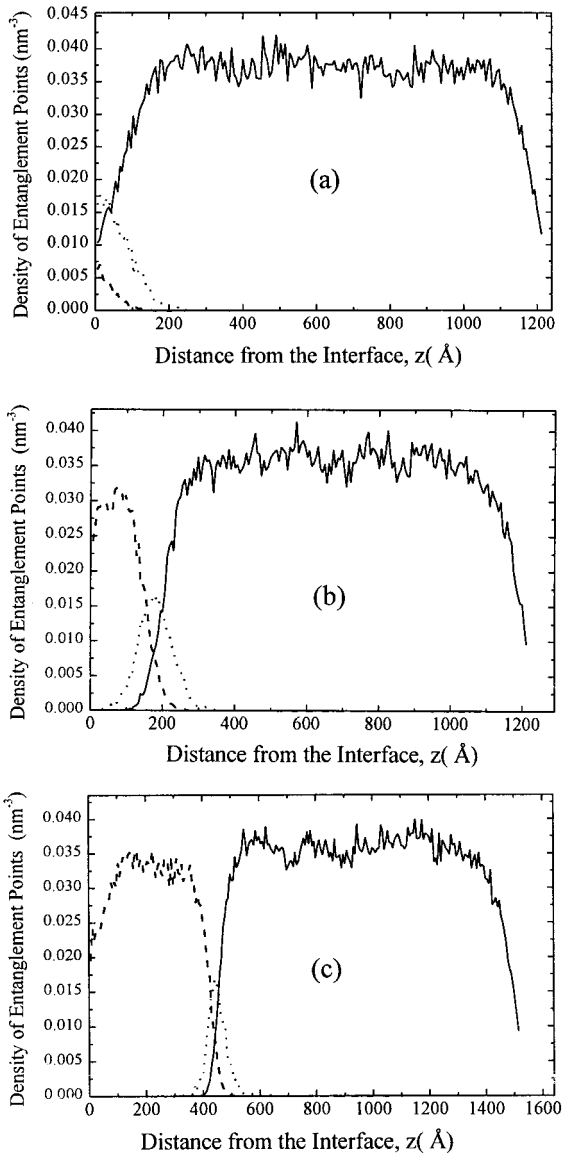

Figure 9. Entanglement density profiles for the generated network, differentiated according to the types of chains involved. Solid line: entanglements between free chains. Dashed line: entanglements between grafted chains. Dotted line: entanglements between grafted and free chains. The correspondence between labeling and surface density is as in the previous figure.

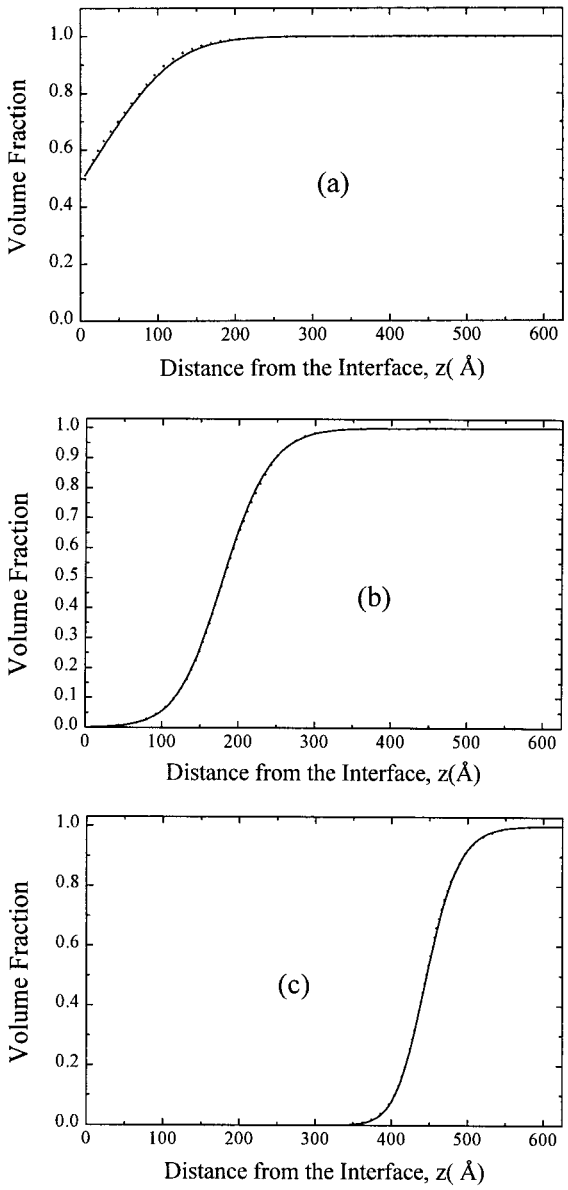

Figure 10. Volume fraction profile of the free chains, as reconstructed after generation of the network (dotted line) and as calculated from the SCF scheme (solid line). The correspondence between plot labels (a−c) and surface density of the grafted chains is as in Figure 8.

men of highest surface density of grafted chains (c). In addition, in both cases b and c there is a small region where entanglements between free and grafted chains contribute the most.

These plots can be used as guides for setting our cutoff for the uniform region of the network. For example, a reasonable cutoff for the network with $\sigma = 0.04$ nm^{-2} is at layer $z = 1100$ Å, and a very good cutoff for the network with $\sigma = 0.50$ nm^{-2} is at $z = 1300$ Å. However, this should not be our unique criterion, as other features (e.g., the end segment volume fractions) could impose smaller cutoffs.

Assuming Gaussian statistics for the density of segments between successive entanglement points, we derive the volume fractions of free and grafted chains. The segment volume fraction profile for free chains is given in Figure 10, as calculated from the SCF model (solid lines) and as obtained from the generated network (dotted line). We observe very good agreement between these two curves for all samples generated. This result suggests that in our network generation we have correctly reproduced the polymer concentrations and conformations in the interfacial region given by the SCF scheme.

The volume fraction profiles for the free ends of grafted chains and for both ends of free chains are given in Figures 11 and 12. The large fluctuations for the network in these plots are due to the small sample size. The profile of the specimen with the lowest surface density (Figure 11a) suggests that the grafted chains, although of contour length 2424 Å, are restricted within a ∼300 Å thick region close to the interface. As the density of grafted chains is increased, they become more extended (Figure 11b). The maximum in the volume fraction of free end segments is seen at about 160 Å. This is very close to the root-mean-square end-to-end distance of a chain of 400 Flory segments, equivalent to 229 Kuhn segments. In this case the conformation of

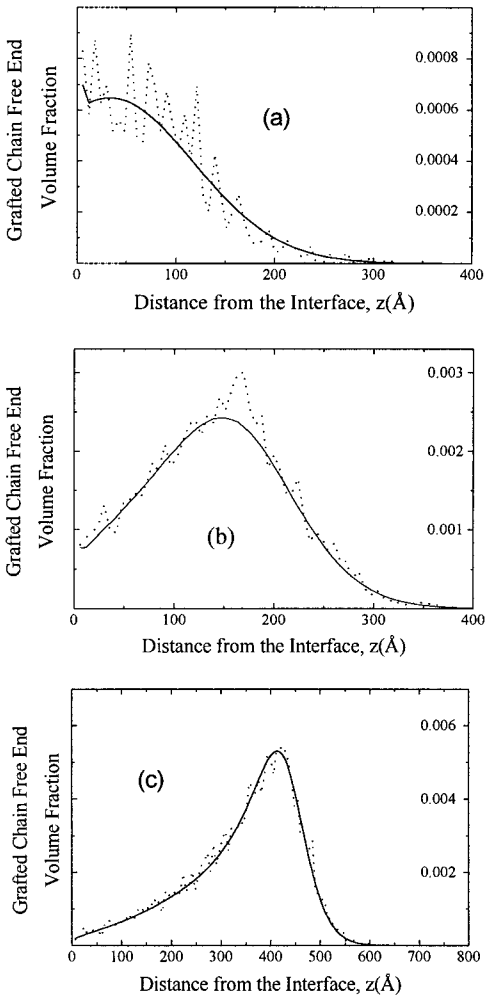

Figure 11. Free end segment volume fraction profile for the grafted chains for the SCF model (solid line) and for the generated network (dotted line). The correspondence between plot labels (a−c) and grafted chain surface density is as in Figure 8.

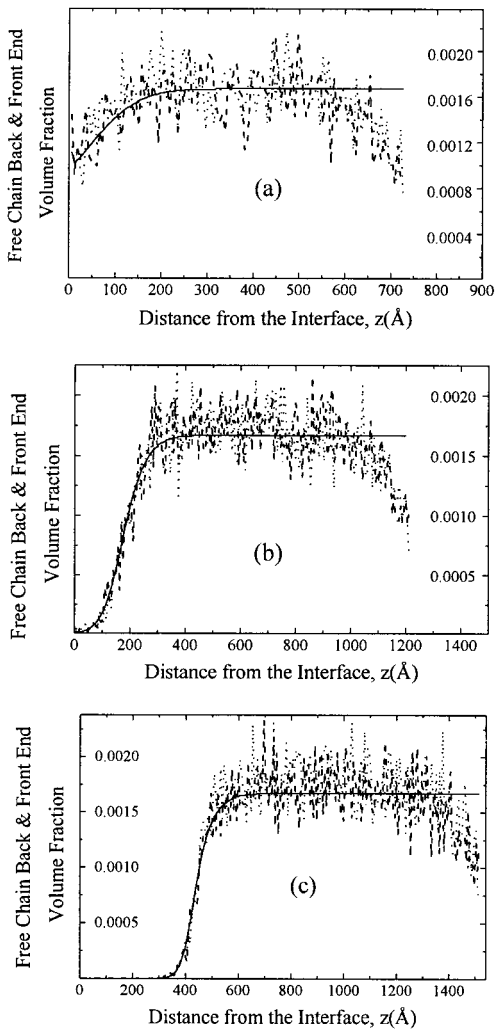

Figure 12. End segment volume fraction profiles for the free chains as obtained from the SCF model (solid line) and from the generated network (dashed and dotted lines). In the network we distinguish between the front end (dashed) and the back end (dotted line) of each chain. The correspondence between plot labels (a−c) and grafted chain surface density is as in Figure 8.

the grafted chains is close to that of "random coils". As the surface density is increased further, the grafted chains become more extended, and their free ends display a sharper peak (Figure 11c). In this case grafted chains are in the "brush" regime. This implies that grafted chains have their tails ordered preferentially perpendicular to the surface (see third column in Table 2 of ref 5). This explains the observed lowering of the entanglement density between pairs of grafted chains and between grafted and free chains (Figure 10c).

The distribution of end points of the free chains (Figure 12a−c) shows a region in which the volume fraction changes from a very low value to a plateau, the width of this region being commensurate with the "random coil" end-to-end distance of a chain of 600 Flory segments. The plateau characterizes the bulk PP region; chain end points have equal probability to appear anywhere in this region. Finally, Figures 10c and 11c clearly indicate that, for high surface grafting density, the region close to the interface is occupied exclusively by grafted chains. The end segment profiles can be a very good indicator for deciding the cutoff layer. Actually, in all but the last case the end segment profiles suggest a shorter cutoff than the entanglement density profile for maintaining a uniform network in the bulk. For example, in the sample with $\sigma = 0.20$ nm^{-2} the cutoff suggested by the entanglement density (Figure 9b) is about 1050 Å, but the one suggested by the end segment volume fractions (Figure 12b) is ca. 50 Å shorter.

We conclude that the placement along the z axis is consistent with the SCF results, provided that our method for generating entanglement networks does indeed conform to the SCF statistical weights.

Structure of the Entanglement Network of the PP/PA6 System. We present results for various molecular weight distributions: (i) monodisperse PP with varying number-average molecular weight, M_n, of 200−800 Flory segments for the grafted chains and M_n of 600 Flory segments for the free chains; (ii) polydisperse PPs with number-average molecular weight $M_n = 400$ Flory segments for the grafted chains and $M_n = 600$ Flory segments for the free chains, both characterized by a variety of molecular weight distributions.

Our values for the average molecular weight have been chosen so as to be comparable to the values of the number-average molecular weight of PP/PA6 samples used in experimental works.[3,4]

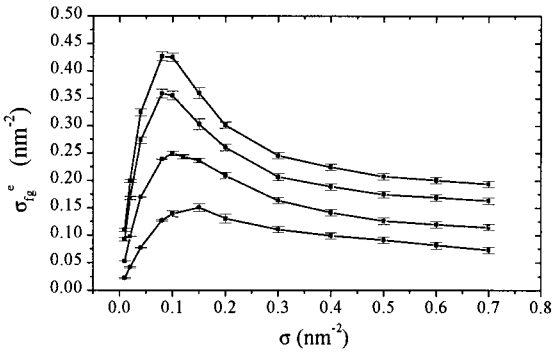

Figure 13. Surface density of entanglements between free and grafted chains, σ^e_{fg}, as a function of the surface density of the grafted chains, σ, for monodisperse specimens with free chains of length $r = 600$ Flory segments. The average chain length of the grafted chains varies between 200 and 800 Flory segments (from bottom to top curve). The entanglement surface density increases systematically with increasing molecular weight of the grafted chains. Error bars are derived from averaging over specimens of various sizes, always larger than (100 Å × 100 Å × 200 Å).

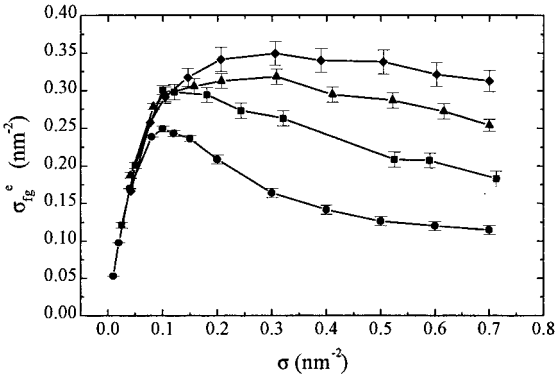

Figure 14. Surface density of entanglements between free and grafted chains as a function of the surface density of the grafted chains for polydisperse samples with number-average length $r = 600$ Flory segments for the free chains and number-average length $r = 400$ Flory segments for the grafted chains. The polydispersity indices are as follows: circles, PDI of free chains = 1.00 and PDI of grafted chains = 1.00; squares, PDI of free chains = 1.04 and PDI of grafted chains = 1.08; triangles, PDI of free chains = 1.04 and PDI of grafted chains = 1.30; diamonds, PDI of free chains = 1.04 and PDI of grafted chains = 1.50. All samples follow a uniform molecular weight distribution.

We are mainly interested in investigating the region where grafted and free chains interentangle. We study the effect of the surface density of grafted chains on the surface density of entanglements (entanglements per unit interfacial area, σ^e_{fg}) between free and grafted chains. These entanglements would be expected to be primarily responsible for adhesion at the interface. When we plot the surface density of entanglements as a function of the surface density of grafted chains (Figures 13−15), a peak appears, which is more pronounced for specimens with grafted chains of high molecular weight and/or low PDI. The observed behavior (existence of a peak in all cases) can be rationalized as follows:

At low surface densities the number of the grafted chains is rather small, and thus the grafted chains are isolated (surrounded mainly by adsorbed free chains) and more or less shaped liked a reflected random walk. Under these conditions, the observed entanglement density σ^e_{fg} is just proportional to the total contour

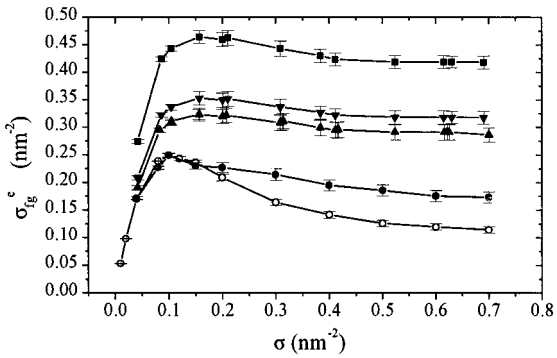

Figure 15. Surface density of entanglements between free and grafted chains, as a function of the surface density of the grafted chains for polydisperse specimens with average length $r = 600$ Flory segments for the free chains and average length $r = 400$ Flory segments for the grafted chains. The molecular weight distributions and polydispersity indices are as follows: open circles, both free and grafted chains are monodisperse; filled circles, PDI of free chains = 1.30 following a uniform distribution and PDI of grafted chains = 1.00; triangles, PDI of free chains = 1.30 and PDI of grafted chains = 1.30, both following a uniform distribution; inverted triangles, PDI of free chains = 1.30 and PDI of grafted chains = 1.30, both following a most probable (Flory) distribution; squares, PDI of free chains = 1.00 and PDI of grafted chains = 2.70, following a Schultz−Zimm (generalized Flory) distribution.

length and hence to the number of grafted chains. A linear behavior between entanglement density and grafting density under constant number-average molecular weight of the grafted chains is expected. For the molecular weights used here, this behavior is seen for densities up to a value that is not very much dependent on the molecular weight (about $\sigma = 0.05$ nm^{-2}).

As the grafting density is increased further, grafted chains come closer to each other. Furthermore, as a result of interchain interactions and exclusion by the interface, they assume more extended conformations. Nevertheless, there is a relatively broad region over which grafted and free chains intermingle. This is the region where a "plateau" of the entanglement density is observed.

As we go to relatively monodisperse samples with even higher surface density, we observe a decrease in the density of entanglements between grafted and free chains, σ^e_{fg}. Obviously, the grafted chains are now so many that they occupy most of region close to the surface, excluding free chains. Only few free chains can penetrate this dense brushlike region in order to create entanglements with the grafted chains. Similarly, few grafted chains penetrate the region where mainly free chains are present. This explanation is supported by Figures 9 and 16, where the profiles of entanglement volume density, ρ^e_{fg}, are shown for the monodisperse case with $r = 400$ Flory segments (for grafted chains). In the caption to Figure 16, in addition to reporting the surface density of the grafted chains, σ, in nm^{-2}, we indicate what fraction of the surface is occupied by grafted chain ends. We calculate this fraction (N/L) as N/L (%) $= 100\sigma$ (in nm^{-2})l_F^2 (in nm^2), where σ is the surface density of grafted chains and l_F the length of the Flory segment. For low grafting densities we observe a decaying profile of entanglements, whose range increases as the surface density is increased. For higher densities entanglements between grafted and free chains

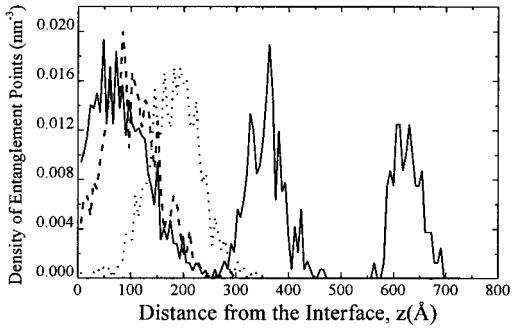

Figure 16. Density profiles of entanglements between free and grafted chains for various surface densities of the grafted chains. The specimen is monodisperse with chain length of 400 Flory segments for the grafted chains and 600 Flory segments for the free chains. The solid lines from left to the right correspond to surface grafting densities of $\sigma = 0.08$ nm^{-2} (2.93% of the first layer occupied by grafted chain ends), $\sigma = 0.40$ nm^{-2} (14.69%), and $\sigma = 0.70$ nm^{-2} (25.71%). The dashed line corresponds to a specimen with $\sigma = 0.10$ nm^{-2} (3.67% of the first layer occupied by grafted chain ends) and the dotted line to a specimen with $\sigma = 0.20$ nm^{-2} (fraction of the surface occupied by grafted chain ends equal to 7.34%).

display a broad bell-shaped profile centered in an intermediate region, which lies between a region fully occupied by grafted chains and a region fully occupied by free chains. The maximum in the total surface density of entanglements ($\sigma^e_{fg} = \int_0^\infty \rho^e_{fg}\, dz$) occurs here when the density profile of Figure 16 occupies the largest "area" (i.e., curve with $\sigma = 0.10$ nm^{-2}). Finally, for very high surface densities the region of free chains is pushed away from the interface. In that case the specimen is mainly composed of grafted chains, and the region of interpenetration between free and grafted chains is narrow and pushed to large distances from the surface.

We have studied the influence of average molecular weight and of polydispersity on the entanglement surface density.

In Figure 13 we observe that increasing the molecular weight of the grafted chains increases the value of the maximum in number of entanglements per unit interfacial area without affecting the surface density of grafted chains at which this maximum value is observed. For given surface density of grafted chains, increasing the molecular weight of the grafted chains causes them to extend further into the region of free chains. This is clearly seen in the three-dimensional visualizations of the entanglement network (see Figures 17 and 18; here strands are represented by rods, and entanglement points and chain ends are represented by spheres).

In Figures 14 and 15 we study the effect of polydispersity on the surface density of the entanglement points between chains of different types. For low surface densities the behavior is independent of the polydispersity of the grafted chains. This is expected; at low surface densities each grafted chain is almost isolated; the final number of the entanglement points of the grafted chains with free chains is proportional to the total grafted chain contour length and thus unchanged if the polydispersity is changed while keeping the number-average molecular weight constant. Polydispersity affects the entanglement structure only at higher surface densities. In this regime a "plateau" is observed, which is higher and more extended for higher values of the polydispersity. In Figure 14 the data points

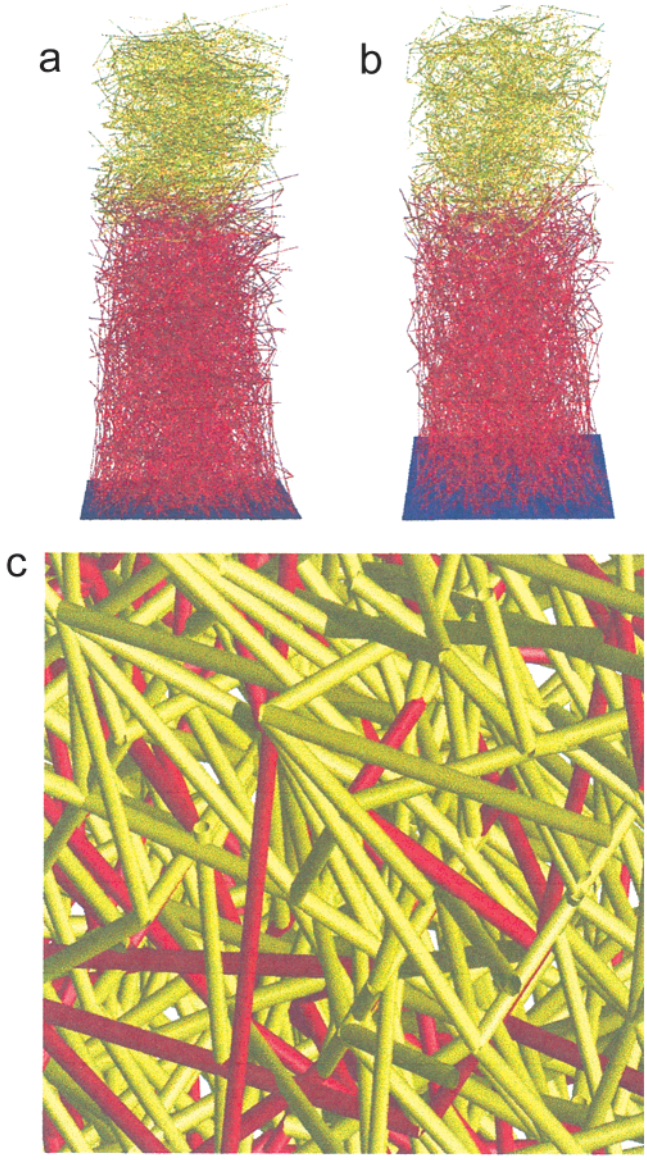

Figure 17. Three-dimensional visualization of an entanglement network with chain length of 400 Flory segments for the grafted chains and 600 Flory segments for the free chains (both monodisperse) and with high surface density of the grafted chains ($\sigma = 0.50$ nm^{-2}). Strands are represented as rods. Grafted chains are represented in red color and free chains in yellow. The specimen consists of 2048 grafted chains and 866 free chains (64 nm × 64 nm × 74 nm). (a) As-generated network upon completion of the entanglement pairing procedure. (b) Relaxed network after conformational free energy minimization. (c) A region of the network close to the interface, magnified significantly (10 nm × 10 nm).

reported correspond to a polydisperse sample, following a uniform distribution. In all cases (PDI = 1.08−1.50) the shortest chain is a monomer. The polydispersity is increased by adding larger chains. The existence of larger chains which can form more entanglements rationalizes the observed increase of σ^e_{fg} for all values of σ.

It is worth pointing out that the entanglement picture described above is in accord with the SCF results. To realize this, we plot in Figure 19 the volume fractions of segments belonging to free and grafted chains, based on our self-consistent field calculations, for two of the cases shown in Figure 16: $\sigma = 0.08$ nm^{-2} (2.93% occupancy of the surface by grafted chain ends) and

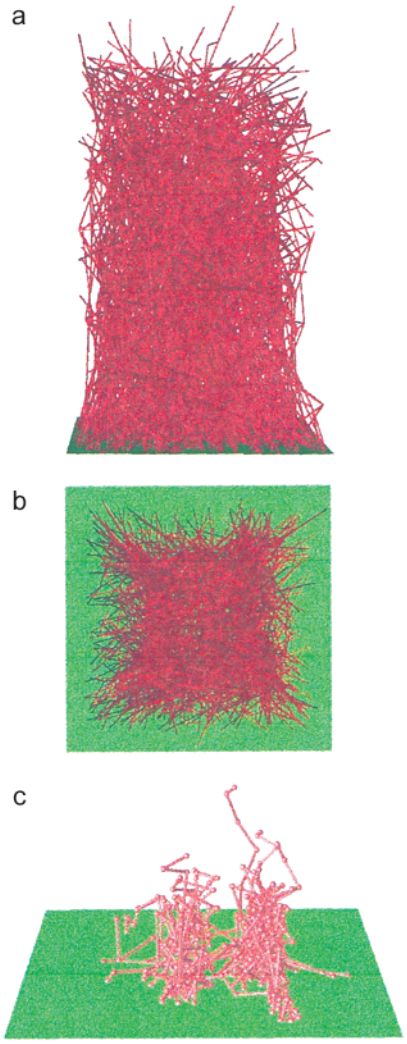

Figure 18. Three-dimensional visualization of entanglement networks. Grafted chains are shown only. (a) View parallel to the interface of a network with chain length of 400 Flory segments for the grafted chains and 600 Flory segments for the free chains (both monodisperse) and with high surface density of grafted chains ($\sigma = 0.50$ nm^{-2}). The number of grafted chains is 2048. The size of the shown region is 64 nm × 64 nm × 48 nm. (b) View of the same network normal to the interface. (c) Network with low surface density of the grafted chains ($\sigma = 0.10$ nm^{-2}). Strands are represented by rods and entanglement points by spheres. The number of grafted chains is 58, and the number of free chains (not shown) is 74. The size of the region occupied by the grafted chains is 24 nm × 24 nm × 12 nm.

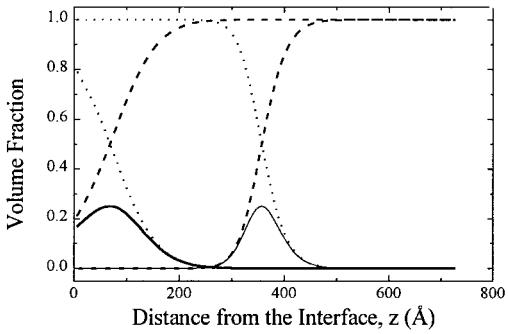

Figure 19. Volume fraction profile of the free chains (dashed lines) and of the grafted chains (dotted lines) for a monodisperse sample with chain length 400 Flory segments for the grafted chains and 600 Flory segments for the free chains. The lines closer to the interface correspond to a grafted chain surface density of 0.08 nm^{-2} (2.93% occupancy of the first layer by grafted chain ends), and the other two lines correspond to a dense sample with grafted chain surface density of 0.40 nm^{-2} (14.69% occupancy of the first layer by grafted chain ends). In the same figure we plot the product $\varphi_g\varphi_f$ of the volume fraction of the grafted chains times the volume fraction of the free chains (solid lines). The integral of this quantity provides an estimate of the extent (width) of the region in which both grafted and free chains coexist.

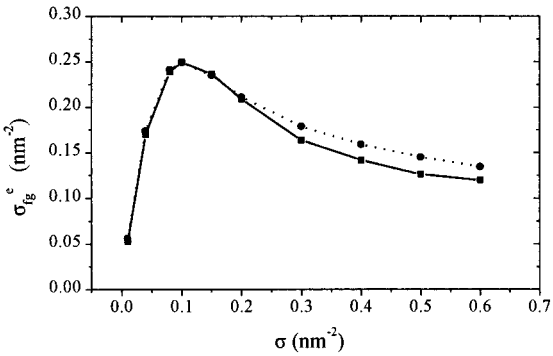

Figure 20. Surface density of entanglements between free and grafted chains as a function of the surface density of the grafted chains for a monodisperse sample with chain length $r = 600$ Flory segments for the free chains and $r = 400$ Flory segments for the grafted chains. The solid line represents data points from generating specimens of various sizes, always larger than (100 Å × 100 Å × 200 Å). The dotted line represents the values of the entanglement surface density as estimated from the width $\int \varphi_{\text{free}}\varphi_{\text{grafted}}\, dz$ through eq 13. To convert from width to entanglement surface density, we multiply by the average entanglement volume density $\bar{\rho}^e$. Here we have used the value $\bar{\rho}^e = 0.0369$ nm^{-3}, which is the average value of entanglement densities used in the generation of various specimens.

$\sigma = 0.40$ nm^{-2} (14.69% occupancy of the surface by grafted chain ends).

We clearly see that the region where both grafted and free chains coexist is broader in the case with the lower (~3%) surface density compared to the case with the higher surface density (~15%).

Along with the volume fractions of the free (dashed line) and grafted (dotted line) chains in Figure 19 we show their product (solid line). By means of this product-($\varphi_g\varphi_f$), we can define an equivalent width of the interface between grafted and free chains as $\int \varphi_g\varphi_f\, dz$. In doing so, we find that this interfacial width is a very good indicator of the entanglement surface density, at least for monodisperse samples (Figure 20). Actually, we can convert the width (derived from the SCF results) to an entanglement surface density provided we have an estimate of the average (volume) entanglement density of the sample we study. For each specific surface density of the grafted chains we use an average entanglement density value $\bar{\rho}^e$, defined as the total number of entanglement points over the volume of the specimen generated (observed values of $\bar{\rho}^e$ range from 0.0364 to 0.0374 nm^{-3}). The entanglement surface density estimated from the SCF results is given by the expression

$$\sigma^e_{fg} = 2\bar{\rho}^e \int \varphi_g\varphi_f\, dz \qquad (13)$$

and is plotted in Figure 20 (dotted line and circular data points). Excellent agreement is observed for low surface density of the grafted chains. For high surface densities the values estimated (from the "SCF" widths) are a bit higher. This is most probably because the SCF-based calculation ignores chain orientation effects which come

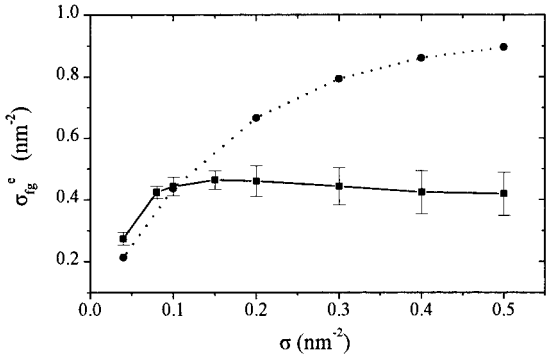

Figure 21. Surface density of entanglements between free and grafted chains as a function of the surface density of the grafted chains for a sample with monodisperse free chains of length $r = 600$ Flory segments and polydisperse grafted chains of number-average length $r = 400$ Flory segments and PDI ∼ 2.7 following a Schultz−Zimm distribution. The solid line tracks results from generating specimens of various sizes, and the dotted line shows estimated values of the entanglement surface density, as derived from the width $\int \varphi_f \varphi_g \, dz$ through eq 13, using $\bar{\rho}^e = 0.0369$ nm^{-3}.

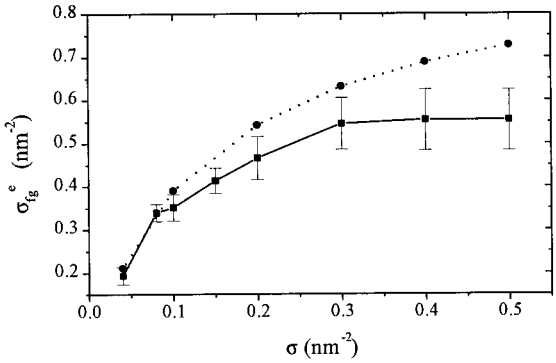

Figure 22. Surface density of entanglements between free and grafted chains as a function of the surface density of the grafted chains for a polydisperse sample with free chains of average length $r = 600$ Flory segments (PDI ∼ 4.7) and grafted chains of average length $r = 400$ Flory segments and PDI ∼ 3.3, both following a lognorm molecular weight distribution. The solid line tracks results from generating specimens of various sizes, and the dotted line shows estimated values of the entanglement surface density, as derived from the width $\int \varphi_f \varphi_g \, dz$ through eq 13, using $\bar{\rho}^e = 0.0369$ nm^{-3}.

into play at high surface grafting densities. It is known (see third column in Table 2 of ref 5) that at high surface density of grafted chains both grafted and free chains are ordered along a direction perpendicular to the interface (positive values of the order parameters). As this ordering is present in the region where the grafted and free chains interentangle, a lowering of the number of entanglements is expected.

In Figure 21 we investigate the more realistic polydisperse case, in which the grafted chains follow a Schultz−Zimm molecular weight distribution with PDI ∼ 2.7. A qualitative difference is observed between the network specimen and the SCF-based predictions for high surface densities of the grafted chains. The entanglement surface density estimated from the SCF width is much higher than that calculated from the generated specimens. This behavior can be understood if we recall that samples following a Schultz−Zimm molecular weight distribution contain a relatively large number of chains of low molecular weight (even monomers), which by definition are incapable of participating in the creation of an entanglement point. The value we use for $\bar{\rho}^e$ in order to estimate σ_{fg}^e matches the value reported from network generation at a grafted chain surface density $\sigma = 0.10$ nm^{-2}. Its use in eq 13 leads to a slight underestimation of the σ_{fg}^e for $\sigma < 0.10$ nm^{-2} and to a gross overestimation of σ_{fg}^e for $\sigma > 0.10$ nm^{-2}.

In Figure 22 we investigate a polydisperse case in which the molecular weight distributions of both grafted and free chains follow a lognorm molecular weight distribution. This is believed to be the most representative of actual PP samples used in experiments.[15] This specimen contains free chains of average length $r = 600$ Flory segments (PDI ∼ 4.7) and grafted chains of average length $r = 400$ Flory segments and PDI ∼ 3.3. It is designed to mimic the sample used in refs 3 and 4. In this case we observe that the entanglement surface density estimated from the SCF width does not deviate very much from that calculated from the generated specimens. This behavior is understood in comparison to the previously studied case of samples following a Schultz−Zimm molecular weight distribution by recalling that, in the lognorm molecular weight distribution, there is a minimum chain length much larger than one Flory segment (here 26 Flory segments). Figures 21 and 22 are in qualitative agreement with the experimental data (refs 3 and 4), as they predict an increase in adhesion at least up to a grafting density of 0.10 nm^{-2}, which is the maximum grafting density that can be achieved experimentally.

4. Conclusions

In the present work we have shown that (a) an interfacial entanglement network can be generated from the distribution functions derived from a self-consistent-field model of a solid/polymer interface strengthened with grafted chains and (b) the conformational and configurational profiles recovered from the generated networks are in agreement with the self-consistent-field theory predictions. In the generation procedure we place entanglement points at equal distances along the contour of each chain. This distance is representative of the experimentally measured molecular weight between entanglements. The placement of nodal points in the direction perpendicular to the surface (z-direction) follows the statistical weights of the SCF theory. The positions of the nodal points of each chain parallel to the interface obey Gaussian statistics. By pairing the nodal points, while at the same time trying to avoid overstretching of chains, a network of entanglement and chain end points is generated. The specimens created in this way are relaxed with respect to the conformation of chain strands between nodes through a Monte Carlo procedure designed to minimize the elastic free energy of the network.

The generation procedure (with the exception of low molecular weight monodisperse samples) is rather time-consuming. The degree of difficulty increases abruptly with the polydispersity index, as for samples of high polydispersity very long chains have to be accommodated within the specimens, strictly following the SCF statistical weights.

Given that the ultimate mechanical properties of the PP/PA6 are to be studied, we are mainly interested in investigating the region where grafted and free chains interentangle. For monodisperse networks, a maximum is observed in the number of entanglements between grafted and free chains per unit area of the interface,

σ^e_{fg}, for some specific value of the surface density of the grafted chains. The maximum is enhanced as the length of the PP chains is increased. In experiments employing monodisperse polymers, this observation would predict that there is an optimal surface density of grafted chains for best adhesion.

Investigating more realistic (at least as regards the PP homopolymer) specimens of high polydispersity indices, we find that the number of free and grafted chains interentanglements per unit surface, σ^e_{fg}, still depends linearly on the grafted chain surface density for low surface densities. Now, however, no peak is observed in σ^e_{fg}; instead, a plateau value is reached for cases of intermediate PDI. For the high PDI (comparable to the PDIs usually reported for PP) samples, a monotonic increase of σ^e_{fg} as a function of the surface density of the grafted chains is seen, toward a plateau value. The information we get from the systematic study of network specimens is shown to be consistent to the predictions of a simple model for the width of grafted and free chains interpenetration based on the SCF density profiles, provided the surface grafting density is not too large.

The procedure followed in this work in order to generate an entanglement network is rather general; it can easily be applied to polymeric systems of different chemical constitution and topology.

Finally, we would like to point out that, although our assumption for the distribution of entanglement points along the contour could be criticized as rather arbitrary and unrealistic, it is a good starting point; currently, there is no experimental information on the distribution of interentanglement spacing along the chains. More information on this distribution is expected to be acquired soon from atomistic simulations.[8]

Acknowledgment. Computational resources for this research were made available by the Educational and Initial Vocational Training Program on Polymer Science and Technology − 3.2a. 33H6. A.F.T. is grateful to DSM Research for financial support.

References and Notes

(1) (a) Creton, C.; Kramer, E. J.; Hui, C.-Y.; Brown, H. R. *Macromolecules* **1992**, *25*, 3075. (b) Washiyama, J.; Creton, C.; Kramer, E. J. *Macromolecules* **1992**, *25*, 5, 4751. (c) Washiyama, J.; Kramer, E. J.; Creton, C. F.; Hui, C.-Y. *Macromolecules* **1994**, *27*, 2019.
(2) Cho, K.; Li, F. *Macromolecules* **1998**, *31*, 7495.
(3) Boucher, E.; Folkers, J. P.; Hervet, H.; Leger, L.; Creton, C. *Macromolecules* **1996**, *29*, 774.
(4) Boucher, E.; Folkers, J. P.; Creton, C.; Hervet, H.; Leger, L. *Macromolecules* **1997**, *30*, 2102.
(5) Terzis, A. F.; Theodorou, D. N.; Stroeks, A. *Macromolecules* **2000**, *33*, 1385.
(6) Schmid, F.; Müller, M. *Macromolecules* **1995**, *28*, 8639.
(7) (a) Tschöp, W.; Kremer, K.; Batoulis, J.; Bürger, T.; Hahn, O. *Acta Polym*. **1998**, *49*, 61. (b) Tschöp, W.; Kremer, K.; Batoulis, J.; Bürger, T.; Hahn, O. *Acta Polym*. **1998**, *49*, 75.
(8) Tsolou, G.; Mavrantzas, V. G.; Theodorou, D. N., manuscript in preparation.
(9) Briels, W., personal communication.
(10) (a) Mark, J. E. *Physical Properties of Polymers*; ACS Professional Reference Book: New York, 1993. See Chapters 1 and 3 therein by W. W. Graessley. (b) Ferry, J. D. *Viscoelastic Properties of Polymers*; John Wiley & Sons: New York, 1980.
(11) Wasserman, S. H.; Graessley, W. W. *Polym. Eng. Sci*. **1996**, *36*, 852. The plateau modulus for atactic polypropylene has been studied by two groups (Pearson, D. S.; Fetters, L. J.; Younghouse, L. B.; Mays, J. W. *Macromolecules* **1988**, *21*, 478. Plazek, D. L.; Plazek, D. J. *Macromolecules* **1983**, *16*, 1469), but the values reported disagree rather substantially. Fetters et al., reexamining their original data, revealed that the value of the plateau modulus reported was too large. The corrected value is in very good agreement with the values reported in the second paper. Subsequent measurements (Fetters, L. J.; Lohse, D. J.; Richter, D.; Witten, T. A.; Zirkel, A. *Macromolecu*les **1994**, *27*, 4639) on other samples indicated a plateau modulus which corresponds to $M_e = 6520$ g/mol. It is worth pointing out that, until the latest work of Fetters et al. appeared in 1994, the entanglement molecular weight reported for atactic polypropylene in several textbooks and research articles was about 2800, i.e., less than half the value currently believed to be true.
(12) Mattice, W. L.; Suter, U. W. *Conformational Theory of Large Molecules*; John Wiley & Sons: New York, 1994.
(13) (a) Zoller, P. *J. Appl. Polym. Sci*. **1979**, *23*, 1051. (b) Rodgers, P. A. *J. Appl. Polym. Sci*. **1993**, *48*, 1061.
(14) Kalos, M. H.; Whitlock, P. A. *Monte Carlo Methods;* John Wiley and Sons: New York, 1986; Vol. I: Basics.
(15) Ir. Markus Bulters and Prof. Costantino Creton, personal communication.

MA991025P